ISSN 2176-5480

22nd International Congress of Mechanical Engineering (COBEM 2013)
November 3-7, 2013, Ribeirão Preto, SP, Brazil

EXPERIMENTAL ANALYSIS AND NUMERICAL MODELING OF PARALLEL PLATE NO-FROST EVAPORATORS

Marco A. S. Timmermann
Jader R. Barbosa Jr.
POLO - Research Laboratories for Emerging Technologies in Cooling and Thermophysics, Department of Mechanical Engineering, Federal University of Santa Catarina, Florianópolis, SC, 88040-900, Brazil
E-mail: jrb@polo.ufsc.br

Abstract. *We present an experimentally validated mathematical model to simulate the thermal behavior of a new type of parallel plate evaporator, which is a potential candidate for substituting tube-fin evaporators in no-frost refrigerators. Experimental results for the air-side thermal conductance were obtained in an open-loop wind-tunnel calorimeter for air flow rates between 17 and 85 m^3/h (10 and 50 ft^3/min). The mathematical modeling consists of dividing the evaporator in a number of control volumes involving the air, plate and coolant domains and solving the coupled energy equations for the three domains to generate local distribuitions of temperature for the air and aluminum plates and enthalpy (temperature) for the refrigerant (coolant). Good agreement was found between the model and the experimental data obtained in the wind tunnel calorimeter.*

Keywords: *Parallel plate heat exchanger, no-frost evaporator, experimental analysis, numerical modeling.*

1. INTRODUCTION

In the so-called 'no-frost' or 'frost-free' refrigerators, aluminum tube-fin heat exchangers are used as evaporators. The geometry of these heat exchangers differs in many aspects from that of more conventional tube-fin heat exchangers. For example, their aspect ratio is such that their face area is smaller and they are comparatively longer (in the air flow direction) than, say, automotive radiators. To avoid flow obstruction due to frosting on the air-side, fin spacing is generally non-uniform and much larger than in conventional tube-fin exchangers. Also, the range of air flow rates tends to be lower than in conventional tube-fin heat exchangers.

Several studies have been performed on the experimental characterization of the air-side heat transfer and pressure drop in 'no-frost' tube-fin evaporators. Karatas *et al.* (1996) tested four evaporator prototypes and assessed the effect of non-uniformities in the temperature and velocity distributions of the inlet air flow. They proposed correlations for the Colburn j-factor and friction factor, and concluded that the former is valid for both the uniform and non-uniform inlet flow cases when mass flow averaged values of temperature and velocity are used at the evaporator inlet. Lee *et al.* (1998) investigated experimentally the effect of fin geometry (e.g., discrete flat plate fins, continuous flat plate fins and spine fins) on the air-side thermal-hydraulic behavior. The spine finned-tube evaporator exhibited the best thermal performance under 'dry' conditions (no condensate or frost formation), with also a significantly lower pressure drop than those of the discrete and continuous flat plate fin geometries. Kim and Kim (2005, 2006) presented experimental data on the air-side heat transfer characteristics of flat plate finned-tube heat exchangers with values of fin pitch between 7.5 and 15 mm. The inline and staggered tube arrays were evaluated, with the number of tube rows varied between 1 and 4. Barbosa *et al.* (2009) carried out experimental tests on eight 'no-frost' evaporator samples to determine the effect of evaporator length (in the flow direction), heat transfer surface area (fin distribution, number of tube rows) and volume of material (mass of aluminum) on the air-side heat transfer and pressure drop. Empirical correlations proposed for the Colburn j-factor and Darcy friction factor, f, correlated the experimental data to within $\pm$ 7% deviation. Barbosa *et al.* (2010) developed an experimentally validated Computational Fluid Dynamics (CFD) model to investigate some aspects of the air-side thermal behavior of tube-fin 'no-frost' evaporators, such as the influence of the defrost heater coils on the air flow distribution and the heat transfer enhancement due to the use of interrupted fins. Waltrich *et al.* (2011) evaluated an alternative 'no-frost' evaporator geometry (the accelerated flow evaporator, AFE) in which the air-side free-flow area is progressively reduced in the direction of the air flow with the objective of increasing the local heat transfer coefficient. Nine AFE prototypes were designed, constructed and tested in an open-loop wind tunnel calorimeter. A mathematical model that enabled the calculation of by-pass flow losses was implemented, yielding a $\pm$ 10% agreement with the heat transfer data.

The purpose of this paper is to investigate the thermal performance of a type of parallel-plate heat exchanger that is an alternative to the tube-fin geometry used in some 'no-frost' refrigerator applications. The main advantages of this evaporator geometry is that they are much simpler from a manufacturing point of view and are easier and safer to install (due to a lower number of soldering spots and absence of sharp edges), thus enabling a reduction of the associated costs.

Experiments were carried out in an open-loop wind-tunnel calorimeter (Barbosa *et al.*, 2009; Waltrich *et al.*, 2011) to determine the air-side thermal conductances of seven prototypes with distinct geometric characteristics for air flow rates between 17 and 85 m^3/h (10 and 50 ft^3/min). The experimental data was employed in the validation of a simplified

ISSN 2176-5480

three-dimensional semi-analytical model for the heat transfer between the air flowing through the parallel plates and the coolant in cross flow through the channels. The model takes into account the variation of the air heat transfer coefficient in the flow developing region and enables the determination of the temperature profile in the plates as a function of position. Agreement between the numerical model and the experimental data are within $\pm$ 10%.

2. EXPERIMENTAL WORK

2.1 Heat exchanger prototypes

Seven heat exchangers were experimentally evaluated in the present work. Figure 1 illustrates their basic geometry. Two 0.5-mm thick symmetric plates with approximately semi-circular embossed grooves are joined together forming a 1-mm thick plate with a particular (i.e., pre-designed) channel pattern. The heat exchanger is formed by roll-folding the single plate so as to form air flow channels between the parallel folds (plates). Table 1 shows the main dimensions and characteristics of the heat exchangers.

Table 1. Summary of the characteristics of the heat exchanger prototypes.

Prototype code	Height [mm]	Width [mm]	Length [mm]	Number of plates (folds)	Air channel thickness [mm]	Number of passes per plate (fold)	Surface area [m^2]
ERNF 1 4F	40	397	150	4	12.0	5	0.476
ERNF 2 4F	50	340	150	4	15.3	5	0.408
ERNF 1 5F	40	397	150	5	8.8	5	0.596
ERNF 3 4F	40	355	154	4	12.0	3	0.437
ERNF 4 3F	30	373	130	3	13.5	5	0.291
ERNF 4 4F	40	385	130	4	12.0	5	0.400
ERNF 4 5F	45	393	130	5	10.0	5	0.511

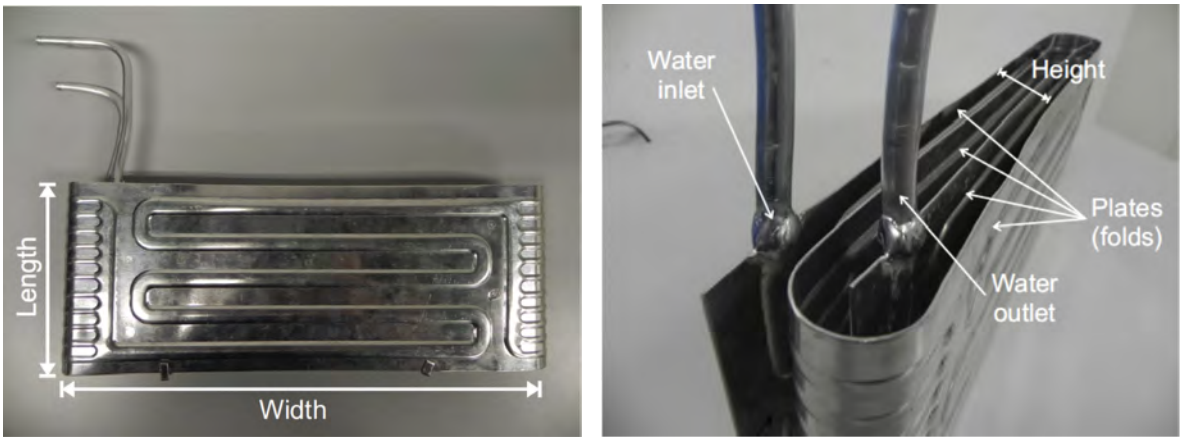

(a) Coolant channels in a plate (fold). (b) Folding of a single plate forming a parallel-plate heat exchanger.

Figure 1. Typical geometry and characteristics of a heat exchanger.

2.2 Experimental facility

The open-loop wind tunnel facility used in the heat transfer tests (Fig. 2) has been described in detail in previous works (Barbosa *et al.*, 2009; Waltrich *et al.*, 2011; Pussoli *et al.*, 2012) and, for completeness, only its main features will be reported here. The facility was constructed from a double layer of steel plates, and a 100-mm thick layer of glass wool was inserted between the plates for thermal insulation. Air flow was supplied by a 51-W variable speed fan, and the flow rate was determined by measuring the pressure drop in a bank of calibrated nozzles. The nozzle pressure drop was measured by a differential pressure transducer with a manufacturer calibration uncertainty of $\pm$0.5% of the full-scale (995 Pa). Wire meshes were employed to make the flow uniform at the inlet and exit sections and also upstream of the air flow nozzles. The air temperature was measured upstream of the heat exchanger by three thermocouples, and downstream of it by six thermocouples. The thermocouples were embedded into small copper blocks (diameter and height of 10 mm) to minimize temperature oscillations during measurements. The temperature fluctuation of the ambient air entering the

ISSN 2176-5480

calorimeter was controlled to ±0.1°C before entering the wind tunnel (Waltrich *et al.*, 2011). The uncertainty of the temperature measurements inside the wind tunnel was ±0.2°C.

A speed-controlled rotary pump, with a maximum flow rate of 4 L/min, drove the water flow inside the tubes. The flow rate was measured with a turbine flow meter with an operating range of 0.4-3.5 L/min and an *in-situ* calibration uncertainty of ± 4.5 mL/min. The water inlet temperature was set by a temperature-controlled bath with an accuracy of ±0.1°C. The water loop was thermally insulated and T-type immersion thermocouples (±0.2°C) were placed immediately upstream and downstream of the heat exchanger.

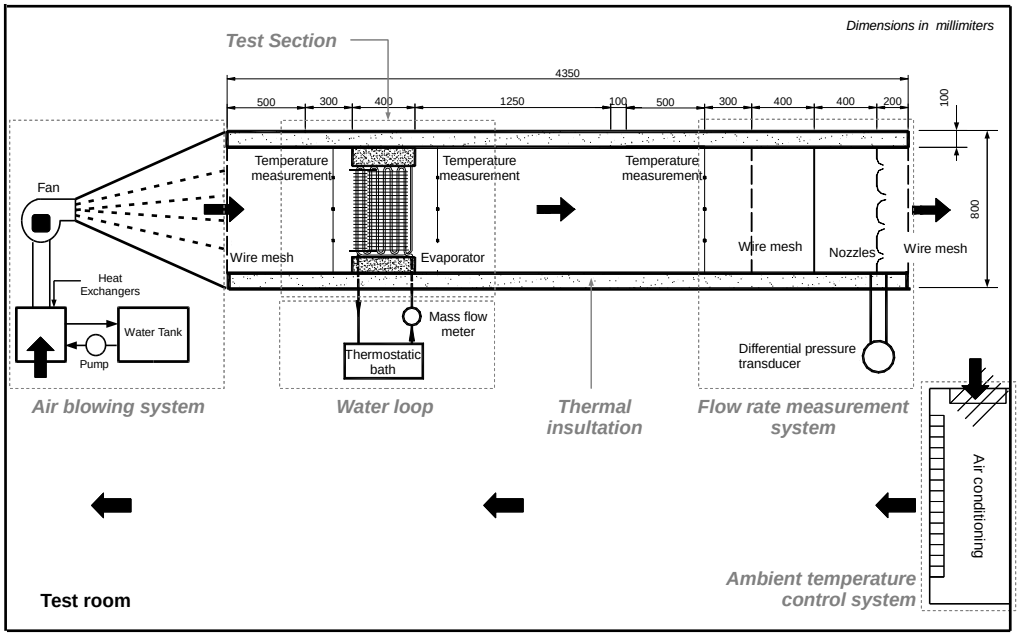

Figure 2. Schematic diagram of the experimental facility (Waltrich *et al.*, 2011).

2.3 Experimental procedure

The experimental procedure is as follows. The inlet water temperature is set to 40°C in the thermostatic bath, and a few minutes are required for it to stabilize. The desired air flow rate is adjusted and the water flow rate is set in order to provide a temperature range (difference between the inlet and outlet temperatures) of 2°C. Five different values of air flow rate are tested between 17 and 85 m^3/h (10 and 50 ft^3/min). The room temperature is set to 20°C ± 1°C. The steady-state criterion has been established so that each variable was averaged over a 30-minute interval. If the absolute value of the difference between the reading at the beginning of the sampling interval (t = 0) and at the end (t = 30 min) was less than 3 times the standard deviation of the signal in that interval, the test was steady.

2.4 Data regression

The experimental air-side heat transfer rate is computed from the following relationship:

$$\dot{Q}_a = \dot{M}_a c_{p,a} \left(\overline{T}_{a,out} - \overline{T}_{a,in} \right) \tag{1}$$

where $\dot{M}_a$ is the total air flow rate, and $\overline{T}_{a,in}$ and $\overline{T}_{a,out}$ are the average air temperatures at the inlet and outlet of the heat exchanger.

The counter-current equivalent overall thermal conductance is given by:

$$UA = \frac{\dot{Q}_a}{\Delta T_{lm}} \tag{2}$$

where:

$$\Delta T_{lm} = \frac{\left(\overline{T}_{r,out} - \overline{T}_{a,in} \right) - \left(\overline{T}_{r,in} - \overline{T}_{a,out} \right)}{\ln \left(\frac{\overline{T}_{r,out} - \overline{T}_{a,in}}{\overline{T}_{r,in} - \overline{T}_{a,out}} \right)} \tag{3}$$

ISSN 2176-5480

3. MODELING

The mathematical model consists of dividing the air and coolant (plates) domains into a number of small control volumes. Figure 3(a) shows a side cross-section view of the parallel-plate heat exchanger illustrating the air passages and the coolant channels in cross-counter flow — see Fig. 3(b). The adiabatic plates above the top plate and below the bottom plate represent the walls of the test section of the wind-tunnel calorimeter, which are assumed to be thermally insulated. Figure 3(b) illustrates the distribution of the channels in a single plate, together with the plate control volumes associated with areas of the plate without a channel. It should be noted that control volumes are assigned to each air channel and parallel plate in the heat exchanger, thus creating a three-dimensional computational domain.

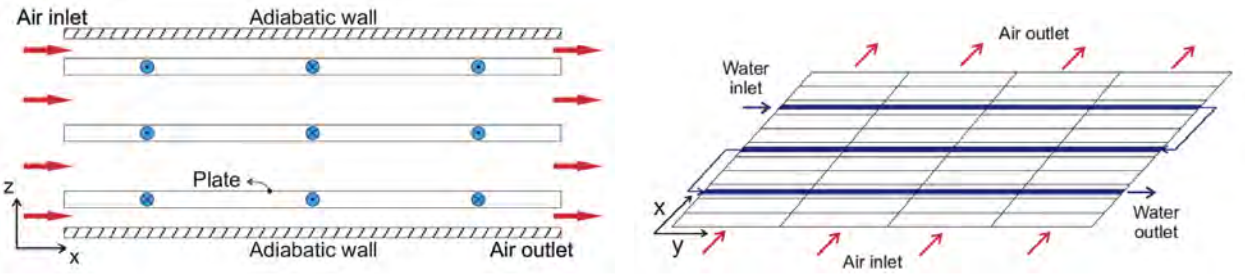

(a) Air flow domain.

(b) Coolant flow and plate domains.

Figure 3. Schematic description of the thermal model domains.

3.1 Thermal model

The following simplifying assumptions have been adopted in the derivation of the balance equations of the mathematical model: (i) Steady state; (ii) uniform wall temperatures in the air flow control volumes; (iii) uniform air temperatures in the coolant and plate control volumes; (iv) constant physical properties; (v) uniform air flow distribution through the plates; (vi) no mass, momentum or energy exchange between adjacent control volumes; (vii) negligible effect of the curvature of the plates on the thermal performance of the evaporator.

3.1.1 Air-side energy balances

Energy balances are needed to compute the air-side heat transfer rates and outlet temperatures associated with each control volume in the air-side domain. The four types of control volume are sketched in Fig. 4. Figure 4(a) shows a control volume limited by two plates, each containing a coolant channel. The control volume of Fig. 4(b) is also sided by two walls, but these correspond to parts of the plates that do not contain coolant channels. The control volumes in Figs. 4(c) and 4(d) are similar to those described previously, but contain an adiabatic wall, thus representing control volumes on the edges of the domain, as can be seen from Fig. 3.

The energy balance in a control volume is given by:

$$\dot{m}_a c_{p,a} dT_a = d\dot{Q}_a \tag{4}$$

where $\dot{m}_a$ is the air mass flow rate in each control volume. For the control volume in Fig. 4(a), the heat transfer rate is given by:

$$d\dot{Q}_a = U_o b\, dx \left[\left(\overline{T}_{r,up} - T_a \right) + \left(\overline{T}_{r,down} - T_a \right) \right] \tag{5}$$

where U_o is an overall heat transfer coefficient (based on the air-side surface area) encompassing thermal resistances between the coolant flow on the inside of the channel and the air flow between the plates, b is the width if the control volume and $\overline{T}_{r,up}$ and $\overline{T}_{r,down}$ are the temperatures of the coolant in the channels in the top and bottom plates. For the control volume in Fig. 4(c), which contains an adiabatic plate and a coolant channel, the heat transfer rate is given by:

$$d\dot{Q}_a = U_o b\, dx \left(\overline{T}_{r,down} - T_a \right) \tag{6}$$

For the control volumes in Figs. 4(b) and 4(d) the heat transfer rates are given by:

ISSN 2176-5480

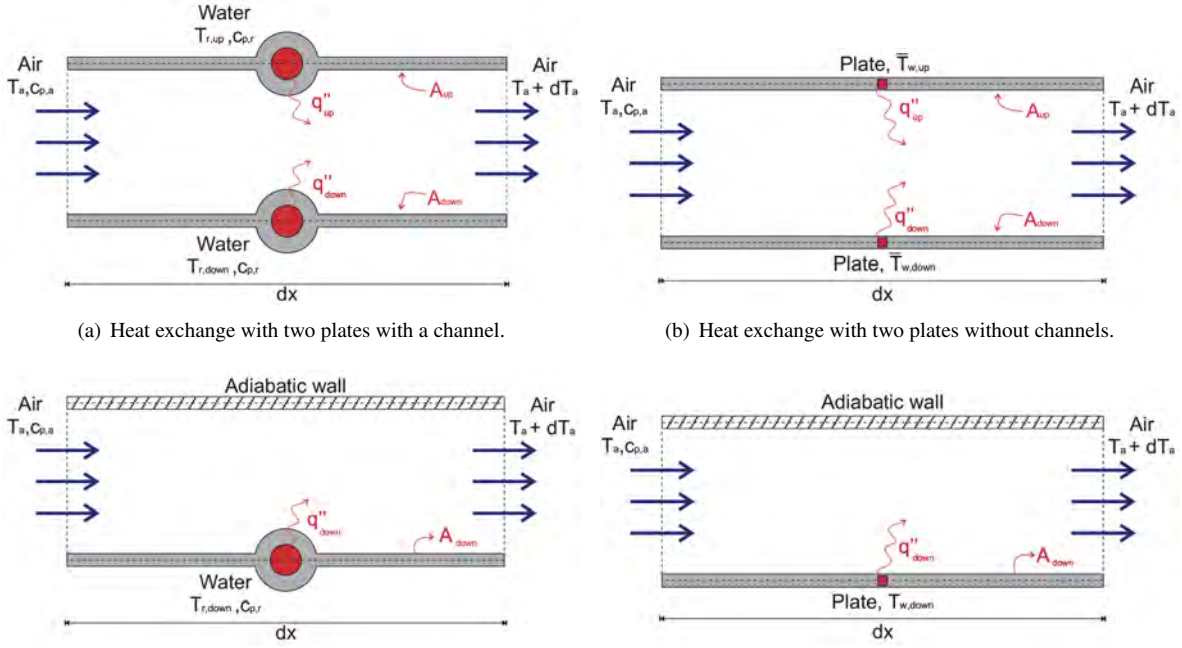

(a) Heat exchange with two plates with a channel.

(b) Heat exchange with two plates without channels.

(c) Heat exchange with only one plate with a channel.

(d) Heat exchange with only one plate without a channel.

Figure 4. Possible types of air-side control volume.

$$d\dot{Q}_a = \hbar_a b\, dx \left[\left(\overline{T}_{w,up} - T_a\right) + \left(\overline{T}_{w,down} - T_a\right)\right] \tag{7}$$

and:

$$d\dot{Q}_a = \hbar_a b\, dx \left(\overline{T}_{w,down} - T_a\right) \tag{8}$$

where $\hbar_a$ is the local air-side heat transfer coefficient and η_o is the overall surface efficiency that accounts for non-uniformities in the plate temperature distribution in the control volume. Combination of Eqs. (5)-(8) with Eq. (4) and integration with $T_a\left(x=0\right) = T_{a,in}$ gives the following relationships for the temperature profiles in each control volume as follows:

$$\frac{1}{2}\left(\overline{T}_{r,up} + \overline{T}_{r,down}\right) - T_a\left(x\right) = \left[\frac{1}{2}\left(\overline{T}_{r,up} + \overline{T}_{r,down}\right) - T_{a,in}\right] \exp\left(-2N_{TU}\frac{x}{L}\right); \quad \text{for control volume 4(a)} \tag{9}$$

$$\frac{1}{2}\left(\overline{T}_{w,up} + \overline{T}_{w,down}\right) - T_a\left(x\right) = \left[\frac{1}{2}\left(\overline{T}_{w,up} + \overline{T}_{w,down}\right) - T_{a,in}\right] \exp\left(-2N^*_{TU}\frac{x}{L}\right); \quad \text{for control volume 4(b)} \tag{10}$$

$$\overline{T}_{r,down} - T_a\left(x\right) = \left(\overline{T}_{r,down} - T_{a,in}\right) \exp\left(-N_{TU}\frac{x}{L}\right); \quad \text{for control volume 4(c)} \tag{11}$$

$$\overline{T}_{w,down} - T_a\left(x\right) = \left(\overline{T}_{w,down} - T_{a,in}\right) \exp\left(-N^*_{TU}\frac{x}{L}\right); \quad \text{for control volume 4(d)} \tag{12}$$

In the above equations, the numbers of transfer units are defined as:

$$N_{TU} = \frac{U_o b L}{\dot{m}_a c_{p,a}} \tag{13}$$

and:

$$N^*_{TU} = \frac{\hbar_o b L}{\dot{m}_a c_{p,a}} \tag{14}$$

ISSN 2176-5480

3.1.2 Coolant-side energy balance

Figure 5 illustrates a control volume for the fluid flow through a channel of the parallel-plate heat exchanger. Heat is transferred to or from the coolant as air flows through the top and bottom surfaces of the plate.

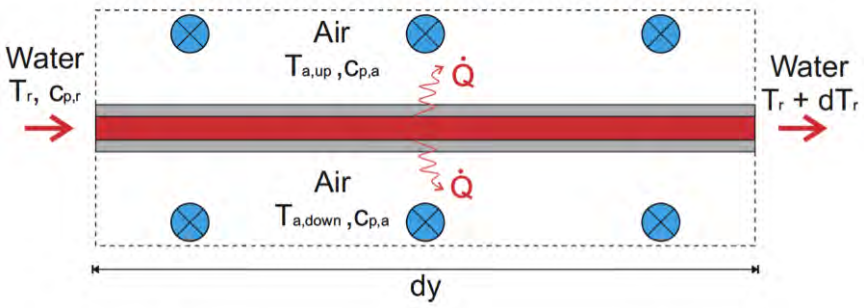

Figure 5. Control volume for the coolant flow in a channel

The energy balance in a coolant control volume is given by (assuming sensible heat transfer only):

$$\dot{m}_r c_{p,r} dT_r = d\dot{Q}_r \tag{15}$$

where $\dot{m}_r$ is the coolant mass flow rate in the channel. For the control volume in Fig. 5, the heat transfer rate is given by:

$$d\dot{Q}_r = U_i \frac{\pi d_i}{2} dy \left[\left(T_r - \overline{T}_{a,up} \right) + \left(T_r - \overline{T}_{a,down} \right) \right] \tag{16}$$

where U_i is an overall heat transfer coefficient (based on the coolant channel surface area) encompassing thermal resistances between the coolant and the air, d_i is the channel diameter. After combining Eqs. (15) and (16) and integrating with $T_r\,(y=0) = T_{r,in}$, the temperature profile in the coolant channel is:

$$T_r\,(y) - \frac{1}{2}\left(\overline{T}_{a,up} + \overline{T}_{a,down} \right) = \left[T_{r,in} - \frac{1}{2}\left(\overline{T}_{r,up} + \overline{T}_{a,down} \right) \right] \exp\left(-N_{TU}^{i} \frac{y}{W} \right) \tag{17}$$

where:

$$N_{TU}^{i} = \frac{U_i \pi d_i W}{\dot{m}_r c_{p,r}} \tag{18}$$

3.2 Overall thermal conductance and heat transfer coefficients

The overall heat transfer coefficients based on the external and internal surface areas in Eqs. (13) and (18) take into account thermal resistances between the coolant and air flows as follows:

$$\frac{1}{U_o} = \frac{1}{\eta_o \hbar_o} + \ln\left(\frac{d_i + 2t}{d_i} \right) \frac{A_o}{2\pi W k_w} + \frac{A_o}{A_i \hbar_r} \tag{19}$$

$$\frac{1}{U_i} = \frac{A_i}{\eta_o \hbar_o A_o} + \ln\left(\frac{d_i + 2t}{d_i} \right) \frac{A_i}{2\pi W k_w} + \frac{1}{\hbar_r} \tag{20}$$

where:

$$A_o = W\left\{ [L - (d_i + 2t)] + \pi\,(d_i + 2t) \right\} \tag{21}$$

$$A_i = \pi d_i W \tag{22}$$

ISSN 2176-5480

The heat transfer coefficient on the coolant side is given by the Gnielinski Nusselt number correlation for turbulent internal forced convection as follows (Lienhard and Lienhard, 2001):

$$Nu_{d_i} = \frac{\hbar_i d_i}{k} = \frac{f/8\left(Re_{d_i} - 10^3\right) Pr}{1 + 12.7\left(f/8\right)^{1/2}\left(Pr^{2/3} - 1\right)} \tag{23}$$

where:

$$f = \left[0.79 \ln\left(Re_{d_i}\right) - 1.64\right]^{-2} \tag{24}$$

The heat transfer coefficient on the air side is calculated using the local Nusselt number relationship for developing flow in parallel-plate channels (Bejan and Kraus, 2003):

$$Nu_{D_h} = 7.55 + \frac{0.024\,\hat{x}^{-1.14}}{1 + 0.0358\,Pr^{0.17}\,\hat{x}^{-0.64}} \tag{25}$$

where $\hat{x}$ is the dimensionless distance from the heat exchanger inlet given by:

$$\hat{x} = \frac{x/D_h}{Re_{D_h} Pr} \tag{26}$$

and $D_h = 2a$, where a is the distance between adjacent plates.

3.3 Plate temperature distribution and surface efficiency

A temperature distribution is developed in the plates as a result of heat conduction and convection to the air. Temperature profiles in the plates are calculated assuming that they behave as rectangular fins with an adiabatic tip, as shown schematically in Fig. 6. Thus, the local temperature in a plate is given by (Lienhard and Lienhard, 2001):

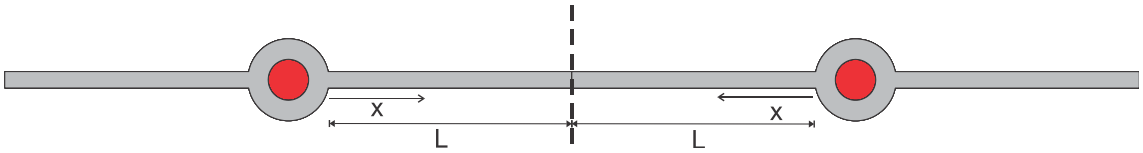

Figure 6. Schematic diagram of adjacent channels with plates acting as fins.

$$\frac{T_w\left(\xi\right) - \overline{T}_a}{T_b - \overline{T}_a} = \frac{\cosh\left[m_f\left(L_f - \xi\right)\right]}{\cosh\left(m_f L_f\right)} \tag{27}$$

where L_f is the fin length and $m_f = \left(\frac{\hbar_a}{k_w t}\right)^{1/2}$. It is assumed that the temperature of the base of the fin is equal to the average coolant temperature in the coolant channel control volume. $\overline{T}_a$ is an average air temperature surrounding the plate. The average plate temperature between two sections ξ_1 and ξ_2 is defined as:

$$\overline{T}_w\Big|_{\xi_1}^{\xi_2} = \frac{1}{\xi_2 - \xi_1}\int_{\xi_1}^{\xi_2} T_w\left(\xi\right) d\xi \tag{28}$$

Thus, integration of the temperature profile gives:

$$\frac{\overline{T}_w - \overline{T}_a}{T_b - \overline{T}_a} = \frac{\sinh\left[m_f\left(L_f - \xi_2\right)\right] - \sinh\left[m_f\left(L_f - \xi_1\right)\right]}{\left(\xi_2 - \xi_1\right) m_f \cosh\left(m_f L_f\right)} \tag{29}$$

The overall surface efficiency needed in Eqs. (19) and (20) is given by:

$$\eta_o = 1 - \frac{A_f}{A_o}\left(1 - \eta_f\right) \tag{30}$$

ISSN 2176-5480

where:

$$A_f = W\left[L - (d_i - 2t)\right] \tag{31}$$

and η_f is the fin efficiency given by (Lienhard and Lienhard, 2001):

$$\eta_f = \frac{\tanh\left(m_f L_f\right)}{m_f L_f} \tag{32}$$

4. COMPUTATIONAL IMPLEMENTATION

The model equations were implemented in the EES (Engineering Equation Solver) software (Klein, 2011). In addition to the geometric parameters associated with each heat exchanger (number of folds, dimensions, coolant channel diameter etc.), the input variables are the inlet temperatures of the two streams and their flow rates. In the present simulations, the number of control volumes per plate was set to 64. Figure 7 illustrates the user interface created in EES (Timmermann, 2013)

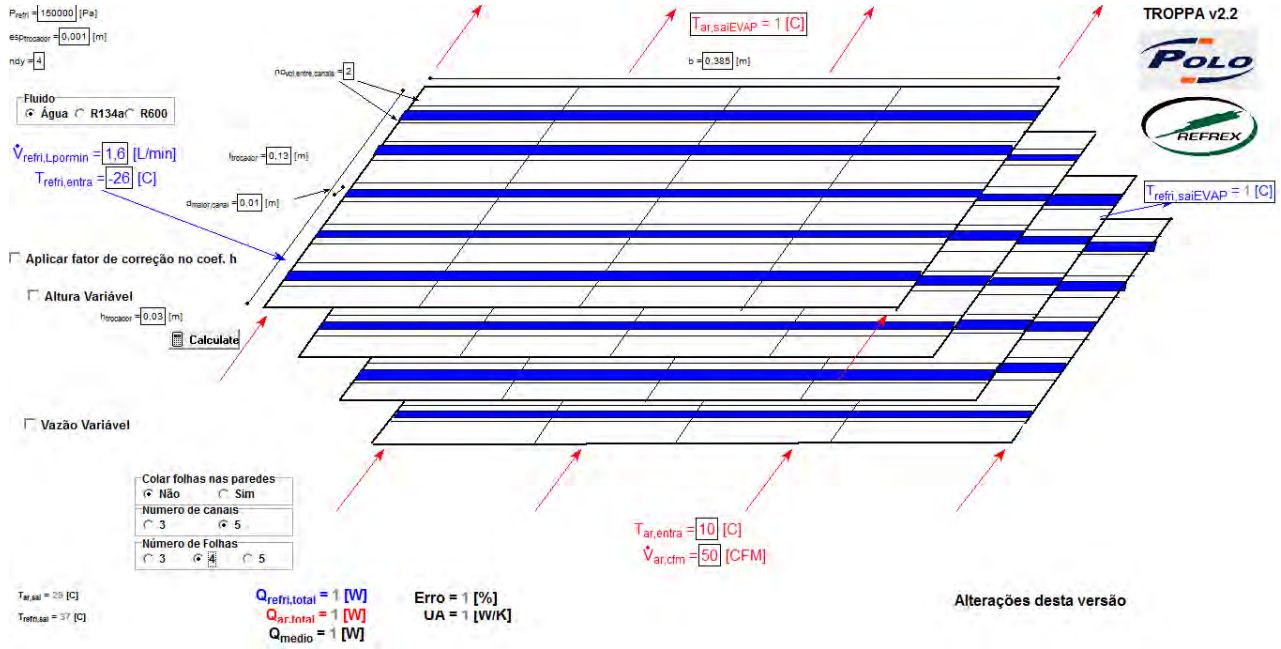

Figure 7. Model user interface in EES.

The solution algorithm is comprised by the following steps:

1. A uniform temperature distribution is assigned to the plates;
2. The air-side energy balances are solved in each control volume. The outlet temperature of a control volume is set equal to the inlet temperature of a control volume downstream of it. The heat transfer rates in each air-side control volume are calculated using the air-side energy balances;
3. With the average air temperature of each air-side control volume, the temperature distribution in the coolant stream is calculated using the coolant-side energy balances. The temperature distribution in the plates is determined via the fin approximation. The heat transfer rates in the coolant control volumes are calculated;
4. If the average absolute deviation between the air-side heat transfer rates in each control volume calculated at successive iterations is larger that 10^{-3}, then return to step 2 until convergence is obtained at each control volume.

5. RESULTS

Figure 8 shows the predictions of the outlet water temperature as a function of the air flow rate for the different heat exchanger samples. A good agreement is observed in general, with a slight underprediction (within the measurement uncertainty) of the experimental data. In almost all cases, the difference between the data and the model were below $0.3°$C, except for the sample ERNF 1 5F for which the deviation at 17 m^3/h was around $0.4°$C.

ISSN 2176-5480

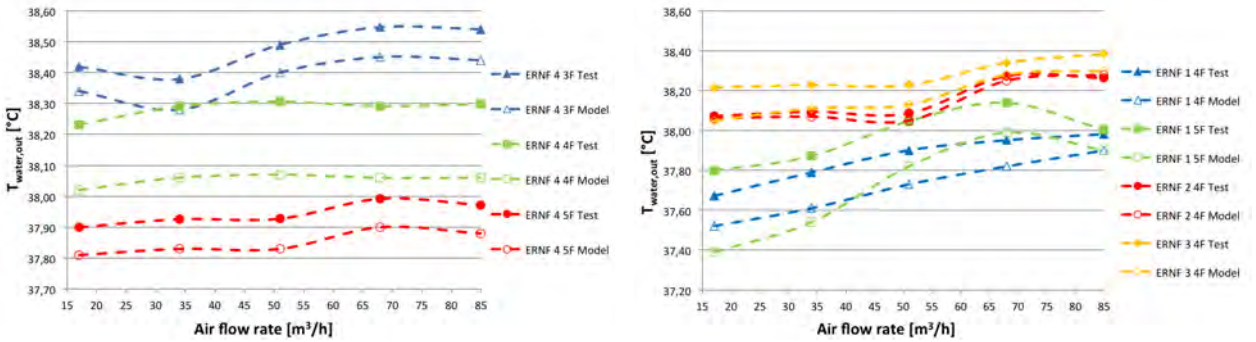

(a) Heat exchangers with a length of 130 mm in the flow direction.

(b) Heat exchangers with a length of 150 mm in the flow direction.

Figure 8. Comparison between model and experiments: water outlet temperature.

Figure 9 shows a comparison between the experimental data and the model predictions of the average outlet air temperature. The average outlet temperature is defined as the mass average of the temperatures leaving the control volumes at the outlet section. As can be seen, a good agreement is also observed, with a general trend for the model to overpredict the data more severely at the lowest air flow rates. This overprediction is more pronounced for the heat exchangers with 5 plates (ERNF 1 5F and 4 5F).

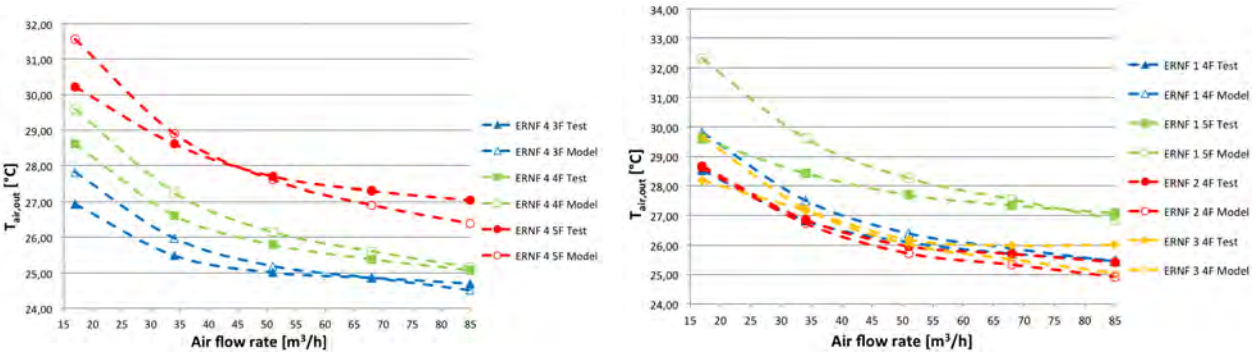

(a) Heat exchangers with a length of 130 mm in the flow direction.

(b) Heat exchangers with a length of 150 mm in the flow direction.

Figure 9. Comparison between model and experiments: air outlet temperature.

Figure 10 shows the results associated with the prediction of the experimental overall thermal conductance calculated with Eq. (2). In general, the trend of the overall thermal conductance of the plate heat exchangers is well picked-up by the mathematical model. In comparison with the conventional tube-fin heat exchangers used as 'no-frost' evaporators (Barbosa *et al.*, 2009), the UA value of the plate evaporators is much smaller (approximately 50%), which is due to the fact that the former has a much higher surface area density due to the presence of fins. As a matter of fact, the plate heat exchanger with the largest UA is ERNF 1 5F, which is the sample with the largest surface area. This confirms previous findings that the surface area is of major importance in determining the thermal conductance in the types of heat exchangers used as evaporators in 'no-frost' appliances.

In order to illustrate the prediction ability of the mathematical model, Fig. 11 shows the variation of the the local heat transfer rate as a function of distance in the direction of the air flow for plate control volumes located at $y = 17.75$ mm (first control volume) and $z = 27$ mm (third plate from the bottom up) for prototype ERNF 3 4F. The air volume flow rate in this case was 51 m^3/h. The general trend is an exponential decay of the local heat transfer rate as a function of x because of the combined decrease of the local air-side heat transfer coefficient (see Fig. 12) and of the coolant-to-air temperature difference. The *spikes* correspond to the control volumes in which the coolant channels are located.

Figure 13 shows the behavior of the overall surface efficiency, η_o, as a function of distance for the same conditions of Figs. 11 and 12. As can be seen, the overall surface efficiency increases mainly as a result of the decrease of the air-side heat transfer coefficient, which increases the fin efficiency.

As seen in the above comparisons, there is an encouraging level of agreement between the data and the model for the majority of the cases. However, it is recognized that the model still has many simplifying assumptions. Sources of discrepancy between the model and the experimental data can be attributed to the curvature of the channels and coolant flow redistribution on the sides of the plates, equivalent surface roughness effects due to coolant channels protruding on the air side and air flow maldistribution between adjacent plates. While the individual and combined influences of these

ISSN 2176-5480

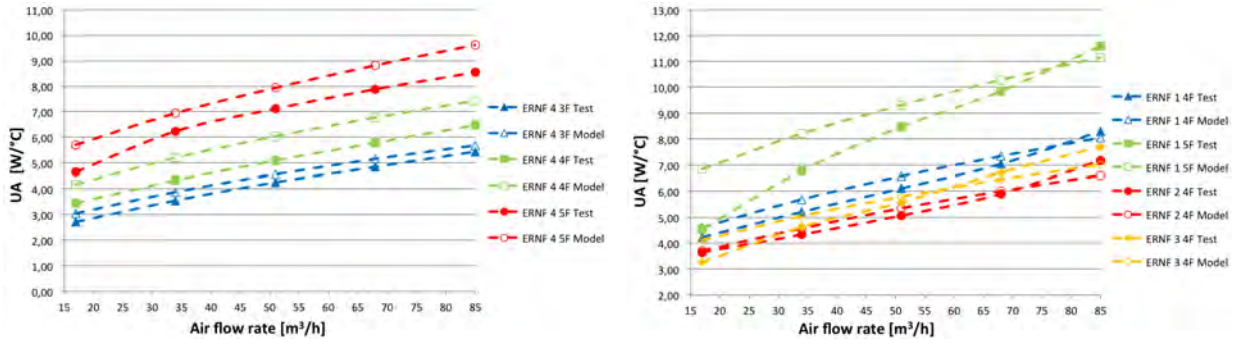

(a) Heat exchangers with a length of 130 mm in the flow direction. (b) Heat exchangers with a length of 150 mm in the flow direction.

Figure 10. Comparison between model and experiments: overall thermal conductance.

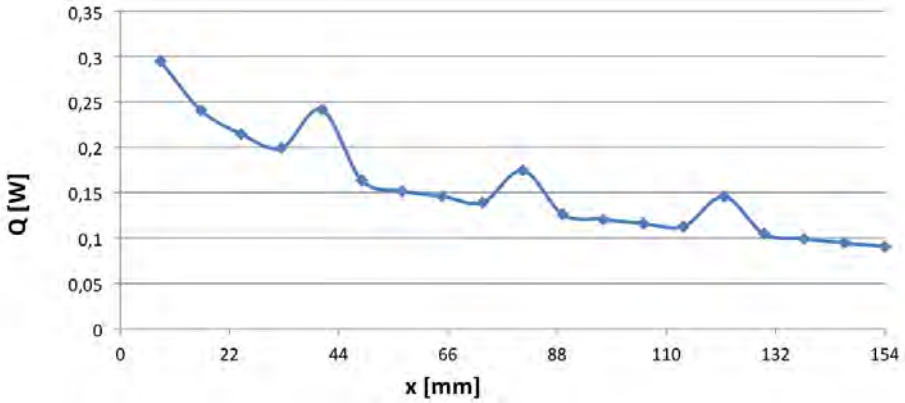

Figure 11. Local heat transfer rate as a function of distance for the prototype ERNF 3 4F.

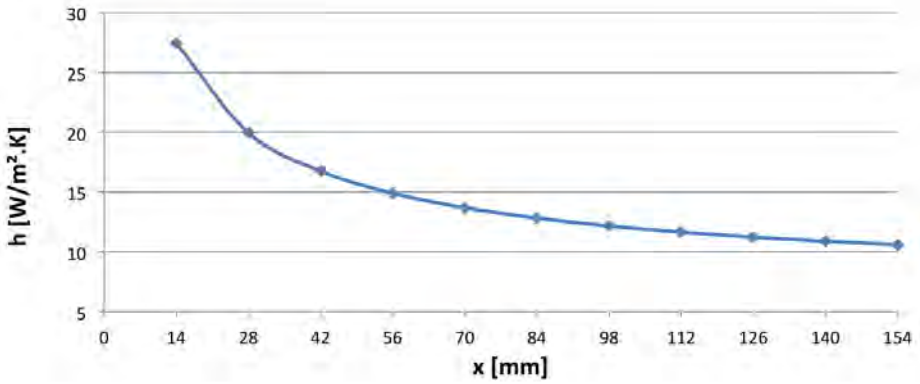

Figure 12. Local air-side heat transfer coefficient as a function of distance for the prototype ERNF 3 4F.

effects on the heat exchanger thermal conductance are difficult to be quantified, air flow maldistribution between plates is certain to contribute negatively to the heat exchanger thermal conductance Jensen *et al.* (2010).

Figure 14 shows temperature profiles on the third plate from the bottom up (at $z = 27$ mm) for prototype ERNF 3 4F for three different air flow rates (17, 51 and 85 m^3/h). The air flow in the figures is from left to right, and the inlet air and water temperatures are 21 and 38.8°C, respectively. The water flow rate was set at 1.7 L/min. The channels are illustrated to facilitate visualization. As can be seen, the plate temperature is close to the inlet air temperature at the leading edge due to the large heat transfer coefficient near the inlet. The plate temperatures are lower for the higher flow rates, also due to the higher heat transfer coefficients.

6. CONCLUSIONS

A simplified three-dimensional semi-analytical model for calculating heat transfer in a new type of parallel-plate forced-flow heat exchanger has been proposed and validated. This new heat exchanger can be used as an evaporator in

ISSN 2176-5480

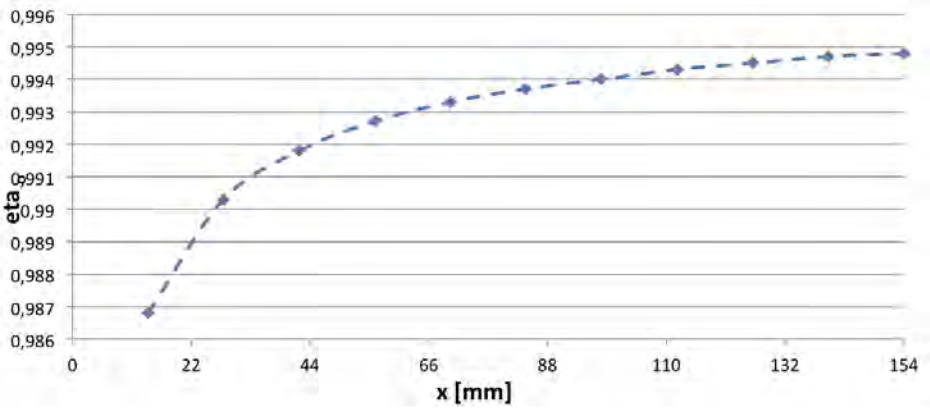

Figure 13. Local overall surface efficiency as a function of distance for the prototype ERNF 3 4F.

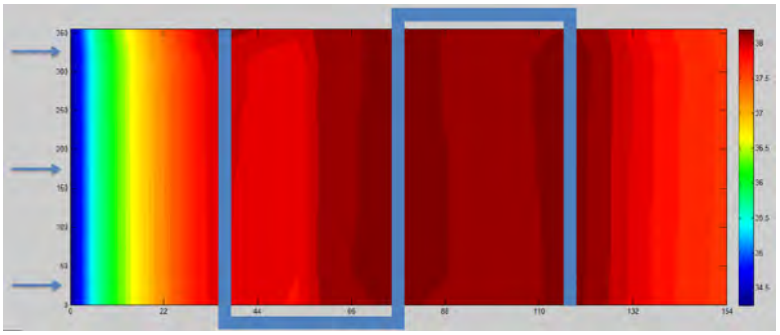

(a) 17 m^3/h.

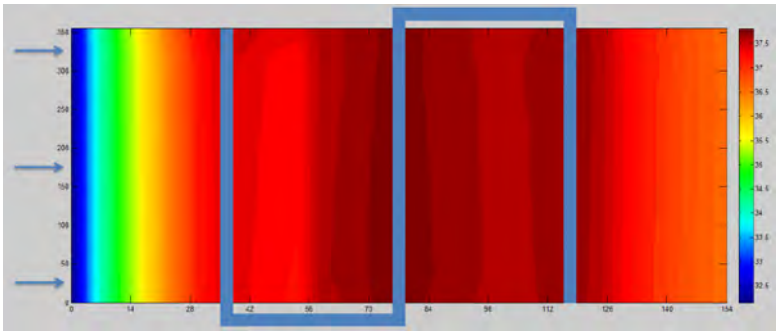

(b) 51 m^3/h.

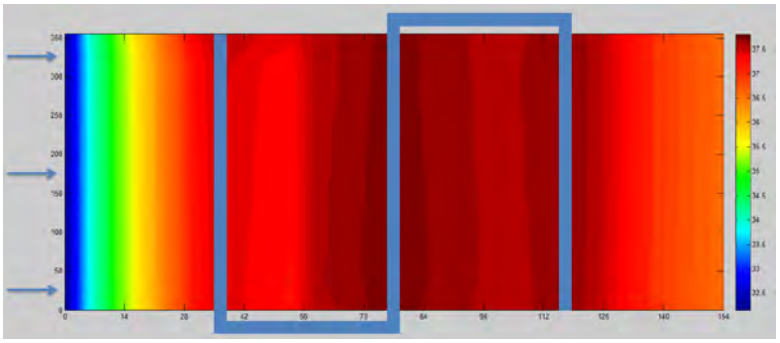

(c) 85 m^3/h.

Figure 14. Plate temperatures for ERNF 3 4F.

'no-frost' refrigerators due to simpler manufacturing and less cumbersome handling and installation. The model combines thermal balances for the developing air flow through the parallel plates and for the coolant in cross flow through channels embossed in the plates. The numerical results were validated against experimental data generated for seven prototypes

ISSN 2176-5480

with distinct geometries using an open-loop wind-tunnel calorimeter. Agreement between the numerical model and the experimental data are within $\pm$ 10% for the overall thermal conductance.

7. ACKNOWLEDGEMENTS

The authors thank Mr. Richard Kaminski (Refrex Evaporadores do Brasil) for supplying the evaporator prototypes used in this study and for the many stimulating technical discussions.

8. REFERENCES

Barbosa Jr., J.R., Hermes, C.J.L. and Melo, C., 2010. "CFD analysis of 'no-frost' evaporators". *Journal of the Brazilian Society of Mechanical Sciences and Engineering*, Vol. 22, pp. 445–453.

Barbosa Jr., J.R., Melo, C., Hermes, C.J.L. and Waltrich, P.J., 2009. "A study of the air-side heat transfer and pressure drop characteristics of tube-fin 'no-frost' evaporators". *Applied Energy*, Vol. 86, pp. 1484–1491.

Bejan, A. and Kraus, A.D., 2003. *Heat Transfer Handbook*. John Wiley & Sons.

Jensen, J.B., Engelbrecht, K., Bahl, C.R., Pryds, N., Nellis, G.F., Klein, S.A. and Elmegaard, B., 2010. "Modeling of parallel-plate regenerators with non-uniform plate distributions". *International Journal of Heat and Mass Transfer*, Vol. 53, pp. 5065–5072.

Karatas, H., Dirik, E. and Derbentil, T., 1996. "An experimental study of air-side heat transfer and friction factor correlations on domestic refrigerator finned-tube evaporator coils". In *8th International Refrigeration and Air Conditioning Conference at Purdue*. West Lafayette, IN.

Kim, Y. and Kim, Y., 2005. "Heat transfer characteristics of flat plate finned-tube heat exchangers with large fin pitch". *International Journal of Refrigeration*, Vol. 28, pp. 851–858.

Kim, Y. and Kim, Y., 2006. "Erratum". *International Journal of Refrigeration*, Vol. 29, p. 336.

Klein, S.A., 2011. "Engineering Equation Solver (EES) Professional Version". V8.819, F-Chart Software, Madison, WI.

Lee, T.H., Lee, J.S., Oh, S.Y., Lee, M.Y. and Lee, K.S., 1998. "Comparison of air-side heat transfer coefficients of several types of evaporators of household freezer/refrigerators". In *9th International Refrigeration and Air Conditioning Conference at Purdue*. West Lafayette, IN.

Lienhard, J.H. and Lienhard, J.H., 2001. *A Heat Transfer Textbook*. Phlogiston Press, 3rd edition.

Pussoli, B.F., Barbosa Jr., J.R., da Silva, L.W. and Kaviany, M., 2012. "Heat transfer and pressure drop characteristics of peripheral-finned tube heat exchangers". *International Journal of Heat and Mass Transfer*, Vol. 55, pp. 2835–2843.

Timmermann, M.A.S., 2013. "Modelagem matemática e análise experimental de trocadores de calor de placas paralelas". Diploma thesis, Department of Mechanical Engineering, Federal University of Santa Catarina.

Waltrich, P.J., Barbosa Jr., J.R., Melo, C. and Hermes, C.J.L., 2011. "Air-side heat transfer and pressure drop characteristics of accelerated flow evaporators". *International Journal of Refrigeration*, Vol. 34, pp. 484–497.

9. RESPONSIBILITY NOTICE

The authors are the only responsible for the printed material included in this paper.